Materials Advances

ROYAL SOCIETY OF CHEMISTRY

PAPER

View Article Online
View Journal | View Issue

Cite this: *Mater. Adv.*, 2024, 5, 274

A tailored polyoxometalate-derived RuW/g-C_3N_4-based electrocatalyst for enhanced hydrogen evolution reaction†

Soyeb Pathan, *[ab] Menon Ankitha, [c] Ajith Arjun Mohan, [d] Neermunda Shabana, [c] Yongfeng Tong [e] and P. Abdul Rasheed *[cd]

Received 15th November 2023,
Accepted 20th November 2023

DOI: 10.1039/d3ma01010d

rsc.li/materials-advances

Graphitic carbon nitride (g-C_3N_4) and its composites for the hydrogen evolution reaction (HER) have gained immense attention owing to their facile synthesis technique and favorable catalytic performance. Herein we present a composite prepared using a g-C_3N_4 and $H_3PW_{12}O_{40}$ polyoxometalate (POM) electrocatalyst synthesized by a novel approach for HER application. The electrocatalyst is synthesized by the complexation of a tailored POM, *i.e.* Ru-substituted polyoxometalate ($PW_{11}Ru$), with melamine followed by calcination under an inert atmosphere. The proposed monomer complexation strategy utilizing well-defined modulated $PW_{11}Ru$ as a metal precursor provided a unique approach for the preparation of a highly dispersed matrix to form a RuW/g-C_3N_4 composite. The HER activity of the obtained RuW/g-C_3N_4 composite is evaluated and compared with individual components of composites by performing several control experiments. RuW/g-C_3N_4 exhibited improved electrochemical activity towards the HER with an overpotential of approximately 266 mV at 10 mA cm^{-2} with a Tafel slope of 63 mV dec^{-1}. This new approach using tailored-transition–metal substituted POMs and melamine as the monomer precursors will be expected to contribute to the development of well-defined cluster-embedded 2D-carbon materials with enhanced electrochemical activities.

Introduction

Hydrogen evolution *via* electrocatalytic water splitting is regarded as one of the foremost encouraging routes to generate energy using environmentally friendly routes.[1–3] Two-dimensional (2D) materials have attracted the curiosity of the research community due to their rich edge states, exceptional conductivity, unique structural properties, subsequent contribution to electron/mass transfer, and relatively low cost in energy applications.[4] Furthermore, the structural morphology and tunable chemical compositions of these materials can be used for targeted function modulations. Various 2D nanostructures including MXenes, graphitic carbon nitride (g-C_3N_4), graphene, and transition-metal dichalcogenides have been evaluated for their electrocatalytic properties with favorable efficiency in the electrolysis of water.[5–12] On comparing with metal clusters or bulk materials, atomically dispersed single-atom or single-atom alloy catalysts are believed to be superior to homogeneous and heterogeneous catalysts.[13] Modifying the metal sites at the atomic level bestows the catalysts with utmost atomic utilization, exceptional electronic properties, improved metal-support interaction, and positive synergy between the active catalytic sites and carbon substrates.[14–16] Despite these advantages, many carbon-based electrocatalytic systems exhibited disadvantages, such as loss of catalytically active sites due to carbon surface destruction under high electrical potentials,[17–19] aggregation of isolated metals caused due to higher mobility of individual metal atoms under harsh reaction conditions, as well as complications associated with the identification of the origin of the catalytic activity and structure–activity relationship.[20,21]

In this context, polyoxometalates (POMs), which are atomically well-defined polynuclear metal oxide anions extend unparalleled opportunities to synthesize atomically dispersed active metal centers.[22–24] Recently, various well-defined

[a] *Research and Development Cell (RDC), Parul Institute of Applied Sciences, Parul University, Waghodia, Vadodara, Gujarat, 391760, India. E-mail: khan_9751@yahoo.com*
[b] *Department of Chemistry, Parul Institute of Applied Sciences, Parul University, Waghodia, Vadodara, Gujarat, 391760, India*
[c] *Department of Chemistry, Indian Institute of Technology Palakkad, Palakkad, Kerala, 678 557, India*
[d] *Department of Biological Sciences and Engineering, Indian Institute of Technology Palakkad, Palakkad, Kerala, 678 557, India. E-mail: abdulrasheed@iitpkd.ac.in*
[e] *Qatar Environment and Energy Research Institute, Hamad Bin Khalifa University, P.O. box 5825, Doha, Qatar*

† Electronic supplementary information (ESI) available: XPS survey spectra, cyclic voltammogram, current density data, ICP analysis and HER polarization curve. See DOI: https://doi.org/10.1039/d3ma01010d

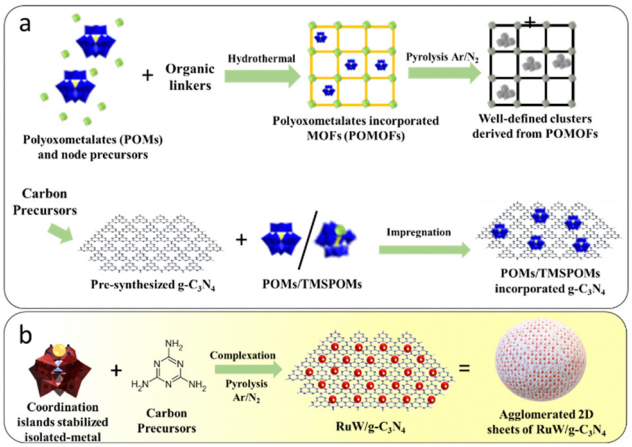

Scheme 1 (a) Various protocols for the synthesis of well-defined nanostructures embedded in a carbon matrix and (b) a monomer complexation approach.

composites of POMs have been reported as efficient electrocatalysts[25–28] as well as precursors for the hydrogen evolution reaction (HER).[29–32] The studies revealed that the presence of POMs assisted in inducing activity in an otherwise inactive counterpart *via* a synergistic effect. POMs incorporated into a 2D-carbon matrix also exhibited enhanced activity in energy applications as compared to the parent materials.[33–36] The high specific surface energy of isolated atoms in the carbon matrix caused easy migration of individual atoms and resulted in agglomerated large clusters. Thus, it would be interesting to attain ''further dispersion'' of the isolated metal center *via* the ''coordination islands'' concept.[37,38] This protocol is expected to minimize or prevent agglomeration of isolated atoms by the incorporation of a metal in lacuna of the POMs to form transition-metal substituted polyoxometalates (TMSPOMs) followed by incorporation to C_3N_4 sites.

Considering these advantages, well-defined bimetallic clusters embedded in carbon catalysts have been developed (Scheme 1(a)) for electrocatalytic applications. Hydrothermal synthesis of a carbon embedded W–Mo heterodimer catalyst, which was derived from TMSPOMs, was synthesized by Zhang and co-workers.[39] The synthesized electrocatalyst exhibited Pt-like HER activity with high stability, showing higher activity than analogous Mo–Mo and W–W homodimer catalysts. Wagberg *et al.* reported electrocatalysts based on carbon-sub-nanometer FeCoW clusters controlled by different TMSPOMs as precursors.[40] Furthermore, multi-step synthesis of single-atom Al and O co-doped Mo_2N quantum dots on conductive N-doped graphene from the well-defined Anderson-typed POM anion clusters ($(NH_4)_3[AlMo_6O_{24}H_6]$) for hydrogen production in alkaline media has also been reported.[41] It is clear that most of the results comprised: (1) the use of a pre-synthesized 2D-carbon matrix for incorporation of either parent POMs or TMSPOMs and (2) hydrothermal synthesis. Furthermore, synthesis using TMSPOMs as precursors for these groups of materials remains unexplored. Thus, there is a need for the simplified synthesis of tailored carbon-materials with the advantage of TMSPOMs derived from well-defined clusters.

Hence, in view of the scarce but encouraging literature reports on the synthesis and electrocatalytic activities of these materials, the possibility of combining well-defined molecular model systems paves the way to designing new atomically dispersed nanostructures embedded in g-C_3N_4 electrocatalysts. Here, g-C_3N_4 incorporated with well-defined RuW clusters through melamine complexation and its atomic-scale modulation of TMSPOM is reported. This is done by synthesizing Ru-substituted phosphotungstate and subsequent calcination under an inert atmosphere (Scheme 1(b)). As far as we are aware, the specified technique has only been used in two publications. The formation of single atoms (arrays) within g-C_3N_4 frameworks by the simple heat treatment of a complex between commercially available $H_4SiW_{12}O_{40}$ and melamine has been reported by Antonietti's group.[42] Recently our group reported g-C_3N_4 incorporated well-defined clusters of RuW derived from Ru-substituted phosphotungstate.[43] Ru was selected for atomic-scale modification of phosphotungstic acid due to its remarkable electrocatalytic activities and relatively low cost compared to Pt (33% less).[44–47] Significantly, the RuW/g-C_3N_4 composite exhibited enhanced electrochemical activity towards the HER in comparison with individual components. The composite showed an overpotential of around 266 mV at 10 mA cm^{-2} with a Tafel slope of 63 mV dec^{-1}.

Experimental

Materials

12-Tungstophosphoric acid, ruthenium trichloride, melamine, sodium dihydrogen phosphate, disodium hydrogen phosphate, sulphuric acid, potassium hexacyanoferrate, acetic acid, sodium bicarbonate, and potassium chloride were purchased from Sigma Aldrich, India.

Synthesis of Ru-substituted phosphotungstate ($PW_{11}Ru$)

Synthesis of $PW_{11}Ru$ was carried out using a reported procedure with slight modification.[48] Briefly, $H_3PW_{12}O_{40}{\cdot}nH_2O$ (PW_{12}; 1 mM) was dissolved in 15 mL of water containing 0.6 mL acetic acid and the pH was adjusted to 5.0 using a saturated sodium bicarbonate solution. $RuCl_3$ (1 mM) was dissolved in the minimum amount of hot water and added to the PW_{12} solution. The final pH of the solution was adjusted to 5.0. The solution was refluxed with stirring for 1 h and the product was filtered. The filtrate was refrigerated overnight. The product was isolated by filtration followed by washing with acetone to obtain brownish-black $PW_{11}Ru$.

Synthesis of RuW/g-C_3N_4

RuW/g-C_3N_4 was synthesized with slight modification in the reported procedure.[43] 0.3 g of $PW_{11}Ru$ was dissolved in the minimum quantity of water and 0.5 g of melamine was added to it and dispersed thoroughly by stirring at 50 °C for 2 h. The final product was washed by centrifugation (5000 rpm; 5 min) with water and dried at 80 °C to obtain a complex of $PW_{11}Ru$ and melamine ($PW_{11}Ru$–Mel). The obtained $PW_{11}Ru$–Mel was

calcined in a tube furnace at 650 °C (with a ramp rate of 2 °C min^{-1}) for 5 h under an inert atmosphere to obtain RuW/g-C_3N_4.

Electrochemical characterization

All electrochemical experiments were performed using a CHI6005 workstation. Initially, the glassy carbon electrode (GCE) was cleaned and 6 μL of the catalyst dispersion (1 mg mL^{-1}) is drop cast on it followed by drying at ambient temperature for 3 h. The cyclic voltammogram (CV) was measured for different electrodes in 0.1 M KCl with 5 mM $[Fe(CN)_6]^{3-/4-}$ at a scan rate of 100 mV s^{-1}. Graphite felt was used as the counter electrode and Ag/AgCl was used as the reference electrode. The polarization curves were measured by performing linear sweep voltammetry (LSV) in 0.5 M H_2SO_4 between 0.1 and −0.7 V and the reference electrode was calibrated against a reversible hydrogen electrode (RHE). The electrochemical active surface area (ECSA) was evaluated by running CV at different scan rates and the durability was evaluated by a continuous 500 CV cycles.

Results and discussion

Material characterization

The Fourier transform infrared (FTIR) spectra (Bruker Alpha II) of pristine melamine, g-C_3N_4, PW_{11}Ru–Mel, and RuW/g-C_3N_4 are presented in Fig. 1. Compared to melamine, the synthesized g-C_3N_4 appears different.[49] FTIR of g-C_3N_4 shows multiple bands in the region 3077–3267 cm^{-1}, 1631 cm^{-1}, and 1204–1565 cm^{-1}, which could be attributed to N–H stretching mode, C═N and C–N, respectively. The PW_{11}Ru–Mel exhibited characteristic bands related to PW_{11}Ru at 1076 and 1036 cm^{-1} – υ_{as} ($P–O_a$), 943 cm^{-1} – υ_{as} ($W–O_b$), 887 cm^{-1} – υ_{as} ($W–O_c–W$), and 853 cm^{-1} – υ_{as} ($W–O_d–W$).[50] The typical bands of melamine appeared with no appreciable shift in wavenumber, suggesting the complexation without any changes happening to the structure of the POM. After calcination under an Argon atmosphere, the synthesized RuW/g-C_3N_4 composites showed the disappearance of several bands of Individual components. The decrease in the number of bands of melamine and PW_{11}Ru may be due to the disintegration of the Keggin unit and the subsequent formation of Ru and W-nanoclusters in the g-C_3N_4 matrix. The FT-IR of RuW/g-C_3N_4 showed a band at 945 cm^{-1} with an additional band at 1233 cm^{-1} that may be due to the W–O and W–C stretching, respectively, indicating the presence of tungsten-oxide and tungsten-carbide phase in RuW/g-C_3N_4. Another band at 802 cm^{-1} corresponding to triazine aromatic repeating units is observed, which confirms the presence of the g-C_3N_4 matrix in the RuW/g-C_3N_4.[51]

Scanning electron microscopy was carried out using a Carl Zeiss Gemini SEM 300. The image of the synthesized g-C_3N_4 (Fig. 2(a)) shows stacked 2D sheets with non-uniform pores. The SEM of PW_{11}Ru–Mel (Fig. 2(b)) displays the typical bulk morphology without any structural characteristics. Interestingly, the composite (RuW/g-C_3N_4) formed by the calcination of melamine in the presence of PW_{11}Ru, *i.e.* calcination of compound (PW_{11}Ru–Mel) synthesized using the monomer complexation approach, exhibits a "poly dispersed spherical" morphology (Fig. 2(c)) as compared to its counterparts. However, evaluation of the SEM images of the composite (Fig. 2(d)) revealed the presence of folded 2D sheets of RuW/g-C_3N_4. Thus, it is predicted that due to high wt% of PW_{11}Ru, the RuW-clusters incorporated 2D-sheets agglomerated together to form an overall non-uniform spherical morphology.

The spherical morphology for the bulk RuW/g-C_3N_4 was further confirmed by transmission electron microscopy (TEM: Tecnai G2, F30) and it is given in Fig. 3(a)–(d), which shows the polydispersed spherical microparticles. Besides, the periphery of dense microstructures shows spicules. For

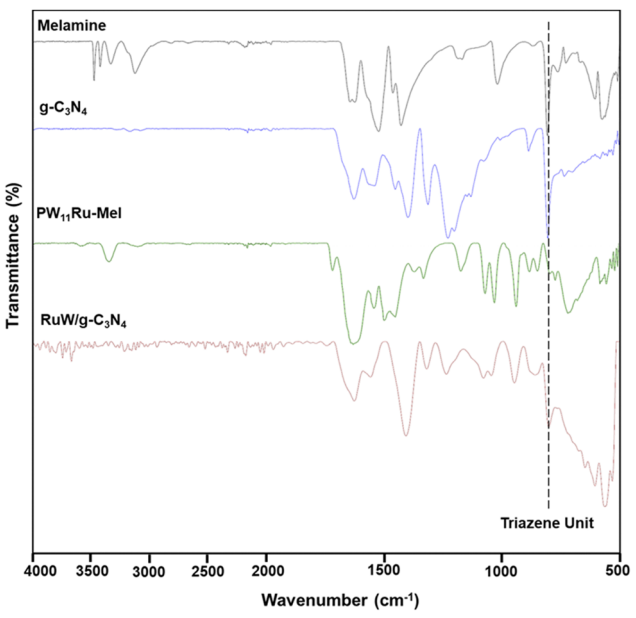

Fig. 1 FT-IR of Melamine, g-C_3N_4, PW_{11}Ru–Mel, and RuW/g-C_3N_4.

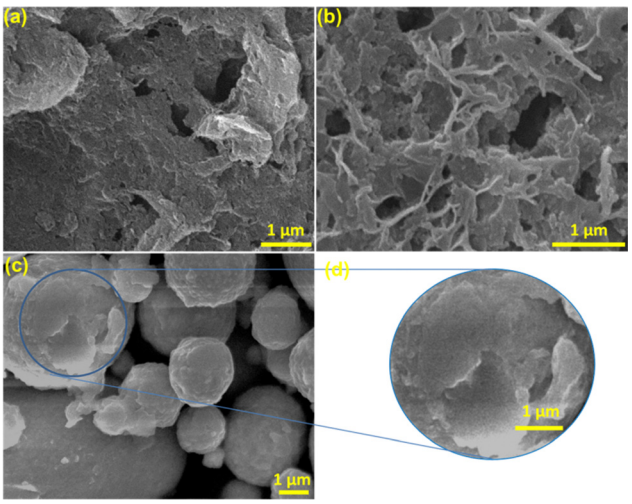

Fig. 2 SEM images of (a) g-C_3N_4, (b) PW_{11}Ru-Mel, and (c) RuW/g-C_3N_4; (d) magnified image of RuW/g-C_3N_4.

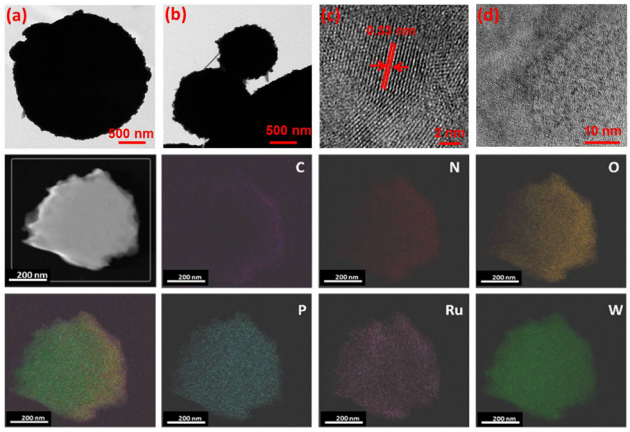

Fig. 3 First raw-TEM images of RuW/g-C_3N_4 for different areas and magnifications (a)–(d); second and third row-STEM and colour mapping of different elements of RuW/g-C_3N_4. All scale bars in the second and third rows correspond to 200 nm.

finer extrapolation of the nanostructure of the composites, the material was subject to ultrasonication for an extended period of 30–40 min before TEM imaging.

The interplanar distance was measured for the composites (Fig. 3(c)) and found to be 0.34 nm corresponding to the (002) plane of g-C_3N_4.[52] At higher magnification (Fig. 3(d)), well-dispersed nano-clusters (<2 nm) of RuW(-oxides) throughout the g-C_3N_4 matrix were observed. This was evident by the elemental mapping of the composite material (Fig. 3), which confirmed the uniform dispersion of elements throughout the g-C_3N_4 matrix. Moreover, no evidence could be observed for the formation of large metal(s) clusters even in the presence of higher W loading. Thus, the described method of complexation is a promising method for the synthesis of well-dispersed metal-centers.

The XRD diffractogram of g-C_3N_4, PW_{11}Ru–Mel, and RuW/g-C_3N_4 is presented in Fig. 4. For g-C_3N_4, the typical peaks at 12.8° and 27.4° correspond to (100) and (002) planes was observed. These peaks can be ascribed to the layered structure

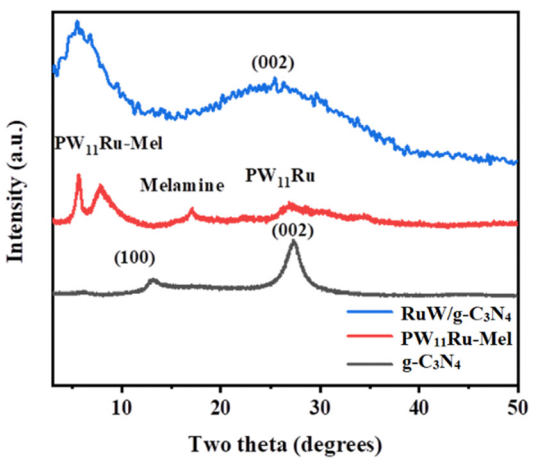

Fig. 4 XRD spectra of g-C_3N_4, PW_{11}Ru–Mel, and RuW/g-C_3N_4.

of the tri-*s*-triazine units[53] and the interlayer stacking of the aromatic system.[53,54] The presence of a Keggin unit in PW_{11}Ru–Mel was confirmed by the sharp peaks in the region 6° and 9° as well as broad peaks in the 25–30° region.[43]

The broadness of the peak suggests the loss of crystallinity of the Keggin structure after the complexation between PW_{11}Ru and the melamine monomer. On calcination of PW_{11}Ru–Mel, the formed RuW/g-C_3N_4 was expected to exhibit a decrease in the number of peaks due to the partial breakdown of the Keggin unit to the corresponding oxide. Thus, RuW/g-C_3N_4 showed a single broad peak in the region 4°–10°. Moreover, the presence of a broad peak with maxima at around 26° confirmed the presence of the g-C_3N_4 matrix in the RuW/g-C_3N_4. Furthermore, no additional peaks of PW_{11}Ru are observed in the region 20–35° and this could be due to the decomposition of the Keggin unit as well as higher dispersion of the corresponding oxides in the g-C_3N_4 matrix.

XPS measurement was conducted on a Kratos Axis Ultra platform with an Alkα X-ray source of 1486.6 eV and a total energy resolution of around 0.1 eV. The measurement is conducted under a UHV of 10–10 mbar at room temperature. A hemisphere analyser with a take-off angle of 90° to the surface is utilized for signal acquisition. The high-resolution (HR) spectra are measured with a step size of 0.1 eV and a pass energy of 10 eV and the wide scan is with a step size of 1 eV and a pass energy of 100 eV. All binding energy positions are calibrated to the C 1s at 284.8 eV (C–C). The XPS survey spectrum of RuW/g-C_3N_4 is shown in Fig. S1 (ESI†) and it indicates the presence of C, N, O, Ru, and W, which is an indication of the presence of g-C_3N_4 and PW_{11}Ru in the composite.[55,56]

Fig. 5 shows the high-resolution (HR) spectra of C 1s, Ru 3d, W 4f and O 1s with deconvolution GL(30) after a proper Shirley background subtraction. Fig. 5(a) shows the C 1s, in which a proper fitting gives 4 related peaks corresponding to the C–C at 284.8 eV, C–O at 286.5 eV, and two N related signals at 287.0 eV

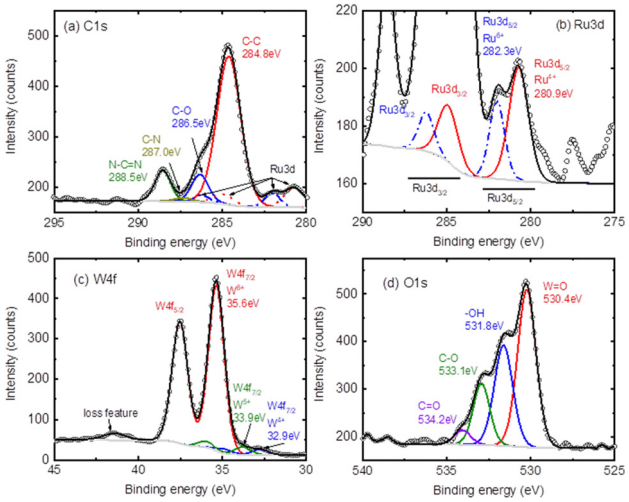

Fig. 5 The core level spectra of (a) C 1s, (b) Ru 3d, (c) O 1s and (d) W 4f of the RuW/g-C_3N_4 composite.

(C–N) and 288.5 eV (N–C=N), respectively.[57–59] Fig. 5(b) presents the Ru 3d with the Ru $3d_{5/2}$ located at 280.9 eV and 282.3 eV for Ru^{4+} (solid-red-line) and Ru^{5+} (dash-blue-line), respectively.[60–62] The related Ru $3d_{3/2}$ are given at 284.9 eV (to 280.9 eV) and 286.4 eV (to 282.3 eV) with a spin-orbital splitting of 4.2 eV (for simplicity the C 1s component was hidden). Fig. 5(c) exhibits the W^{6+} valence state with the W $4f_{7/2}$ located at 35.6 eV, which corresponds to the W–O bond.[63,64] A blue doublet with W $4f_{7/2}$ at 32.9 eV and a green doublet at 33.9 eV can be assigned to the W^{4+} and W^{5+} states, which can probably be assigned to the W–C bond.[29,64] A loss feature at the higher BE side of 41.4 eV is also observed, which is a signature of the W^{6+} states.[65–69] This again confirms the presence of WO_3 in the composites. The corresponding O 1s signal is given in Fig. 5(d), where the different oxidation components, including the W–O/Ru–O at 530.4 eV, the metal hydroxide (M–OH) at 531.8 eV, the carbon related C–O at 533.1 eV and the carbonate (O–C=O) at 534.2 eV, can be distinguished.[70] The O 1s indicates the possible $Ru_xW(OH)_y$ species in the composites.

Inductively coupled plasma (ICP) analysis was carried out to evaluate the concentration of Ru and W in the RuW/g-C_3N_4 composite and it was found that the percentage of Ru is only 3.7 and the concentration of W is around 59.5% (Table S1, ESI†). This shows that the presence of Ru in the final composite is much less. In addition, we have made Ru/g-C_3N_4 and W/g-C_3N_4 composites with the ratio of 3.7 and 59.5% of Ru and W respectively by simply mixing g-C_3N_4 with salts of Ru and W to compare the HER performances.

Electrochemical analysis

The RuW/g-C_3N_4 modified GCE was evaluated and compared with the RuW and g-C_3N_4 modified GCE for its electrochemical performance. Fig. S2 (ESI†) shows the CV of different modified electrodes in which the peak currents of the GCE increased considerably by 30–40 μA for both anodic and cathodic peaks after modification with $PW_{11}Ru$ and g-C_3N_4. The peak current is further enhanced by 20–30 μA for the RuW/g-C_3N_4 modified GCE. The large surface area and promising electrical conductivity of the composite could accelerate the electron transfer rate and enhance the HER performance.

The HER activities of the RuW/g-C_3N_4 samples were studied in 0.5 M H_2SO_4 solution with a specific amount of sample loaded on a GCE and compared with a bare GCE and Pt/C. As shown in Fig. 6(a), the GCE showed very weak electrocatalytic activity while the Pt/C showed the best HER activity. The onset overpotential of Pt/C is approximately 7 mV, and the overpotential is 69 mV (at 10 mA cm^{-2}). The overpotential of $PW_{11}Ru$ was 446 mV while the corresponding value of g-C_3N_4 is 427 mV. However, the overpotential of the RuW/g-C_3N_4 composite was 266 mV, which is around 40% lower than the HER overpotential of g-C_3N_4 and around 37% lower than the HER overpotential of $PW_{11}Ru$. These results showed that the HER performance of the RuW/g-C_3N_4 composite is significantly better compared to its individual components. In addition, at the same overpotential of 266 mV, the current density of RuW/g-C_3N_4 is 10 mA cm^{-2}, which is higher

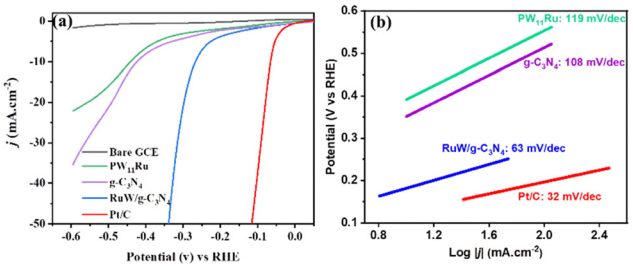

Fig. 6 (a) HER polarization curve and (b) the corresponding Tafel plots of $PW_{11}Ru$, g-C_3N_4, and RuW/g-C_3N_4 composites in comparison with Pt/C.

than that of $PW_{11}Ru$ (2.7 mA cm^{-2}) and g-C_3N_4 (3.69 mA cm^{-2}) (Fig. S3, ESI†).

The Tafel slopes of $PW_{11}Ru$, g-C_3N_4, and the RuW/g-C_3N_4 composite are given in Fig. 6(b) by fitting the linear portion of the polarization curves. The Tafel slope for Pt/C (32 mV dec^{-1}) is lower than all samples for commercial Pt/C. The Tafel slopes for $PW_{11}Ru$ and g-C_3N_4 are 119 mV dec^{-1} and 108 mV dec^{-1}, respectively. The Tafel slope for the composite is 63 mV dec^{-1}, which is much lower than that of pure g-C_3N_4 and $PW_{11}Ru$ and it confirms that the incorporation of $PW_{11}Ru$ on g-C_3N_4 can significantly enhance the electrocatalyst performance. Here, the enhanced HER performance of RuW/g-C_3N_4 arises due to the Ru metal centers embedded on the g-C_3N_4 backbone, which can enhance the HER performance. A comparison table showing the HER performance of POM/g-C_3N_4-based catalysts is presented in Table 1. The HER performance of the RuW/g-C_3N_4 composite is comparable with the reported Ru-based POM materials, with a Tafel slope of 63 mV dec^{-1} even with a lower content of Ru (only 3.7%).

As control experiments, the HER performances of the Ru/g-C_3N_4 and W/g-C_3N_4 composites were compared with RuW/g-C_3N_4 and the results are given in Fig. S4 (ESI†). As shown in Fig. S4 (ESI†), the HER activity of these composites is much less compared to RuW/g-C_3N_4. It shows that there is appropriate synergy between the precursor and g-C_3N_4 matrix during the monomer complexation approach, while it is not observed in Ru/g-C_3N_4 and W/g-C_3N_4 composites. The control experiments confirm the improved activity as compared to their counterparts, *i.e.* Ru/g-C_3N_4, suggesting synergy between Ru and W in RuW/g-C_3N_4 catalyzed HER. Thus, Ru and W both are predicted as active sites and the electronic interactions between these two metals can catalyze the hydrogen evolution.[71] In addition, the presence of WO_3 can transfer free electrons to Ru, which results in an interfacial electric field and this electron-rich region on the Ru surface can enhance the binding capability with protons.[72,73] Moreover, WO_3 in an acidic environment can form a hydrogen tungsten bronze compound (H_yWO_3) through H insert/insert out, which results in hydrogen transfer from the active site to the WO_3 substrate.[73,74]

To evaluate the interactions between $PW_{11}Ru$ and the g-C_3N_4 matrix quantitatively, charge-transfer resistance (R_{ct}) and electrochemical active surface area (ECSA) were utilized. Fig. 7(a) shows the CVs of RuW/g-C_3N_4 at different scan rates and it

Table 1 Comparison showing the HER performance of POM/g-C_3N_4 based catalysts

Material	Overpotential@10 mA cm^{-2} (mV)	(Tafel slope) (mV dec^{-1})	Ref.
Co-WS_2/P-$WO_{2.9}$	146 and 120 (acidic and alkaline)	86 and 74 (acidic and alkaline)	75
$\{Cu_2(3\text{-bptzp})_3(H_2O)_4[SiW_{12}O_{40}]\}H_2O$ (Keggin-type)	59.4 (alkaline media)	74 (alkaline media)	76
Co_2P/WC@NC/CNTs	171 and 198, (0.5 M H_2SO_4, 1.0 M KOH),	65 and 42 (acidic and alkaline)	77
$[PW_{11}MO_{39}]_5$-@Ru-rGO	−0.41 and −1.65 (*vs.* Ag/AgCl) (acidic and alkaline)	36.56, 107.95 (acidic and alkaline)	78
POM derived Co/WN	143 (both acidic and alkaline media)	90 and 118 (acidic and alkaline)	79
Ru-MoO_2@PC	230 (alkaline)	86.6 (alkaline)	80
Ru doped WO_3	124 (acid)	28, 17.6, and 83 (acidic, alkaline, and neutral)	81
2D $[Co_2(TIB)_2(PMo_{12}O_{40})]\cdot Cl\cdot 4H_2O$	137 mV (acidic)	59 (acidic)	82
CoW_{12}/clicked g-C_3N_4	230	67	83
g-C_3N_4-boron nitride and chitosan	520 (acidic)	150 (acidic)	84
RuW/g-C_3N_4	266 (acidic)	63 (acidic)	This work

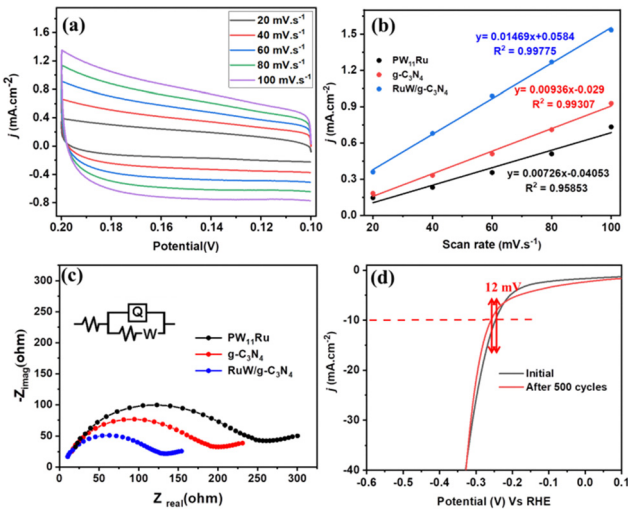

Fig. 7 (a) CVs of GCE modified with RuW/g-C_3N_4 in the range of 0.1–0.2 V at different scan rates. (b) Variation of double layer charging current at +0.15 V *vs.* scan rate for the GCE modified with $PW_{11}Ru$, g-C_3N_4, and the RuW/g-C_3N_4 composite. (c) Nyquist plot for the GCE modified with $PW_{11}Ru$, g-C_3N_4, and the RuW/g-C_3N_4 composite. (d) The first and 500th cycle of HER polarization curve of the GCE modified with the RuW/g-C_3N_4 composite after 500 cycles of cyclic voltammetry experiments in the potential window of −0.6 to 0.2 V.

shows that the current density increases with scan rate. The slope of the current density at −0.15 V and scan rate (Fig. 7(b)) provides double-layer capacitance (C_{dl}), which can be used as proportional to ECSA. The C_{dl} of RuW/g-C_3N_4 was calculated as 14.7 mF cm^{-2}, which was 1.56 times that of g-C_3N_4 (9.36 mF cm^{-2}), and 2 times that of $PW_{11}Ru$ (7.26 mF cm^{-2}). This increase in C_{dl} value confirms the enhanced electrical conductivity of the composite due to the incorporation of metal centers into the g-C_3N_4 matrix.

The R_{ct} values were measured from electrochemical impedance measurements. Fig. 7(c) depicts the typical Nyquist plots of $PW_{11}Ru$, g-C_3N_4, and the RuW/g-C_3N_4 composite, and the R_{ct} value was assessed (inset of Fig. 7(c)). The R_{ct} values are lower for the RuW/g-C_3N_4 (145 Ω) composite in comparison with $PW_{11}Ru$ (258 Ω) and g-C_3N_4 (190 Ω) and this corresponds to enhanced electron transfer kinetics of the composite, which is corroborated by the CV data. In addition, the stability of the catalysts is also evaluated, which is an important parameter when considering practical applications. The polarization curve showed a negligible difference of 12 mV after 500 scan cycles in the onset potential (Fig. 7(d)). This negligible difference in the overpotential confirms the long-term stability of the catalyst even in the absence of a binder molecule.

The present work aimed to simplify the preparation of bimetallic-supported C_3N_4 from tailored POM. Due to the known remarkable electrocatalytic activities of Ru, we have decided to use Ru for the substitution of one of the W from phosphotungstate. We believe that a simplified approach will be useful for developing similar bimetallic catalytic systems with different transition metals. This protocol has numerous advantages, such as straight forward synthetic route, the privilege of module metallic compositions as POMs can be designed at the molecular level, low-cost reagents, non-hydrothermal conditions, and no use of organic templates (in the case of MOF-derived nanoclusters).

Conclusion

In summary, the present synthesis protocols demonstrated the development of well-defined RuW-clusters embedded in a 2D-C_3N_4 matrix *via* straightforward monomer complexation. Furthermore, FT-IR, SEM and TEM showed retention of 2D-C_3N_4 in the composites. The presence of individual elements as well as composition was confirmed by TEM-mapping and XPS analysis. TEM mapping showed uniform dispersion of Ru and W throughout the matrix, without agglomeration of metallic clusters. XPS analysis also revealed the presence of two types of W (based on oxidation states), associated with W–O and W–C bonds in addition to the Ru–O bond. The HER catalytic activity of the RuW/g-C_3N_4 composite was evaluated and compared with $PW_{11}RuO_{40}$, g-C_3N_4, Ru/g-C_3N_4, W/g-C_3N_4 and Pt/C. The RuW/g-C_3N_4 composite exhibited improved electrochemical activity towards the HER with an overpotential of approximately

266 mV at 10 mA cm^{-2} with a Tafel slope of 63 mV dec^{-1}. The novel approach using tailored-TMSPOMs and melamine as the monomer precursors is expected to contribute to the development of other base-metal-derived well-defined cluster-embedded 2D-carbon materials with enhanced electrochemical activities.

Author contributions

Conceptualization-SP, PAR; formal analysis-MA, AMA, NS; investigation-SP, PAR, YT; methodology-SP; supervision-SP, PAR; validation-MA, AMA, PAR; writing – original draft-MA, NS, AMA, YT; writing – review & editing-SP, PAR.

Conflicts of interest

There are no conflicts to declare.

Acknowledgements

SP acknowledges Parul University for financial support (IMR: CR4D/IMSL/053 dated 11/02/2022). PAR acknowledges the Ramalingaswami re-entry fellowship (BT/RLF/Re-entry/75/2020) from the Department of Biotechnology (DBT), Govt. of India. The authors are thankful to SAIF, IIT Bombay and CIF, IIT Palakkad for characterization facilities. We acknowledge the Nanotechnology Research Centre (NRC), SRIMST for providing the XPS analysis facility.

Notes and references

1 M. S. Dresselhaus and I. L. Thomas, *Nature*, 2001, **414**, 332–337.
2 J. A. Turner, *Science*, 2004, **305**, 972–974.
3 Q. Xue, X.-Y. Bai, Y. Zhao, Y.-N. Li, T.-J. Wang, H.-Y. Sun, F.-M. Li, P. Chen, P. Jin, S.-B. Yin and Y. Chen, *J. Energy Chem.*, 2022, **65**, 94–102.
4 Q. Zhu, Y. Qu, D. Liu, K. W. Ng and H. Pan, *ACS Appl. Nano Mater.*, 2020, **3**, 6270–6296.
5 S. Intikhab, V. Natu, J. Li, Y. Li, Q. Tao, J. Rosen, M. W. Barsoum and J. Snyder, *J. Catal.*, 2019, **371**, 325–332.
6 R. Meshkian, M. Dahlqvist, J. Lu, B. Wickman, J. Halim, J. Thörnberg, Q. Tao, S. Li, S. Intikhab, J. Snyder, M. W. Barsoum, M. Yildizhan, J. Palisaitis, L. Hultman, P. O. Å. Persson and J. Rosen, *Adv. Mater.*, 2018, **30**, 1706409.
7 Y. Qu, Y. Ke, Y. Shao, W. Chen, C. T. Kwok, X. Shi and H. Pan, *J. Phys. Chem. C*, 2018, **122**, 25331–25338.
8 J. Wen, J. Xie, X. Chen and X. Li, *Appl. Surf. Sci.*, 2017, **391**, 72–123.
9 K. Geethalakshmi, T. Y. Ng and R. Crespo-Otero, *J. Mater. Chem. C*, 2016, **4**, 8429–8438.
10 R. J. Toh, Z. Sofer, J. Luxa, D. Sedmidubský and M. Pumera, *Chem. Commun.*, 2017, **53**, 3054–3057.
11 H. Liang, H. Shi, D. Zhang, F. Ming, R. Wang, J. Zhuo and Z. Wang, *Chem. Mater.*, 2016, **28**, 5587–5591.
12 H. Pan, *Sci. Rep.*, 2014, **4**, 5348.
13 X.-F. Yang, A. Wang, B. Qiao, J. Li, J. Liu and T. Zhang, *Acc. Chem. Res.*, 2013, **46**, 1740–1748.
14 S. Ji, Y. Chen, X. Wang, Z. Zhang, D. Wang and Y. Li, *Chem. Rev.*, 2020, **120**, 11900–11955.
15 A. Wang, J. Li and T. Zhang, *Nat. Rev. Chem.*, 2018, **2**, 65–81.
16 G. Yilmaz, S. B. Peh, D. Zhao and G. W. Ho, *Adv. Sci.*, 2019, **6**, 1901129.
17 D. Zhao, Z. Zhuang, X. Cao, C. Zhang, Q. Peng, C. Chen and Y. Li, *Chem. Soc. Rev.*, 2020, **49**, 2215–2264.
18 X. X. Wang, M. T. Swihart and G. Wu, *Nat. Catal.*, 2019, **2**, 578–589.
19 F. M. Oliveira, I. Danylo, V. Mazánek, M. Veselý, R. Gusmão and Z. Sofer, *Mater. Adv.*, 2022, **3**, 4348–4358.
20 M. J. Hülsey, J. Zhang and N. Yan, *Adv. Mater.*, 2018, **30**, 1802304.
21 R. Qin, P. Liu, G. Fu and N. Zheng, *Small Methods*, 2018, **2**, 1700286.
22 M. J. Hülsey, V. Fung, X. Hou, J. Wu and N. Yan, *Angew. Chem., Int. Ed.*, 2022, **61**, e202208237.
23 M. J. Hülsey, G. Sun, P. Sautet and N. Yan, *Angew. Chem., Int. Ed.*, 2021, **60**, 4764–4773.
24 D. Zang and H. Wang, *Polyoxometalates*, 2022, **1**, 9140006.
25 C. Singh, A. Haldar, O. Basu and S. K. Das, *Inorg. Chem.*, 2021, **60**, 10302–10314.
26 D. Jana, H. K. Kolli, S. Sabnam and S. K. Das, *Chem. Commun.*, 2021, **57**, 9910–9913.
27 D. M. Fernandes, M. P. Araújo, A. Haider, A. S. Mougharbel, A. J. S. Fernandes, U. Kortz and C. Freire, *ChemElectroChem*, 2018, **5**, 273–283.
28 R. Liu, G. Zhang, H. Cao, S. Zhang, Y. Xie, A. Haider, U. Kortz, B. Chen, N. S. Dalal, Y. Zhao, L. Zhi, C.-X. Wu, L.-K. Yan, Z. Su and B. Keita, *Energy Environ. Sci.*, 2016, **9**, 1012–1023.
29 X.-L. Wang, Y.-J. Tang, W. Huang, C.-H. Liu, L.-Z. Dong, S.-L. Li and Y.-Q. Lan, *ChemSusChem*, 2017, **10**, 2402–2407.
30 Y. Hou, H. Pang, L. Zhang, B. Li, J. Xin, K. Li, H. Ma, X. Wang and L. Tan, *J. Power Sources*, 2020, **446**, 227319.
31 Z. Zeb, Y. Huang, L. Chen, W. Zhou, M. Liao, Y. Jiang, H. Li, L. Wang, L. Wang, H. Wang, T. Wei, D. Zang, Z. Fan and Y. Wei, *Coord. Chem. Rev.*, 2023, **482**, 215058.
32 Z.-Y. Tian, X.-Q. Han, J. Du, Z.-B. Li, Y.-Y. Ma and Z.-G. Han, *ACS Appl. Mater. Interfaces*, 2023, **15**, 11853–11865.
33 J. Miao, Z. Lang, X. Zhang, W. Kong, O. Peng, Y. Yang, S. Wang, J. Cheng, T. He, A. Amini, Q. Wu, Z. Zheng, Z. Tang and C. Cheng, *Adv. Funct. Mater.*, 2019, **29**, 1805893.
34 X.-L. Zhai, J. Liu, L.-Y. Hu, J.-C. Bao and Y.-Q. Lan, *Chem. – Eur. J.*, 2018, **24**, 15930–15936.
35 R. Gong, D. Mitoraj, D. Gao, M. Mundszinger, D. Sorsche, U. Kaiser, C. Streb, R. Beranek and S. Rau, *Adv. Sustainable Systems*, 2022, **6**, 2100473.
36 Y. Gao, Z. Lang, F. Yu, H. Tan, G. Yan, Y. Wang, Y. Ma and Y. Li, *ChemSusChem*, 2018, **11**, 1082–1091.
37 R. Liu and C. Streb, *Adv. Energy Mater.*, 2021, **11**, 2101120.
38 A. Kondinski and T. N. Parac-Vogt, *Front. Chem.*, 2018, **6**, 346.

39 Y. Yang, Y. Qian, H. Li, Z. Zhang, Y. Mu, D. Do, B. Zhou, J. Dong, W. Yan, Y. Qin, L. Fang, R. Feng, J. Zhou, P. Zhang, J. Dong, G. Yu, Y. Liu, X. Zhang and X. Fan, *Sci. Adv.*, 2020, **6**, eaba6586.
40 X.-B. Han, X.-Y. Tang, Y. Lin, E. Gracia-Espino, S.-G. Liu, H.-W. Liang, G.-Z. Hu, X.-J. Zhao, H.-G. Liao, Y.-Z. Tan, T. Wagberg, S.-Y. Xie and L.-S. Zheng, *J. Am. Chem. Soc.*, 2019, **141**, 232–239.
41 Y. Huang, W. Zhou, W. Kong, L. Chen, X. Lu, H. Cai, Y. Yuan, L. Zhao, Y. Jiang, H. Li, L. Wang, L. Wang, H. Wang, J. Zhang, J. Gu and Z. Fan, *Adv. Sci.*, 2022, **9**, 2204949.
42 B. Kumru, D. Cruz, T. Heil and M. Antonietti, *Chem. Mater.*, 2020, **32**, 9435–9443.
43 N. Shabana, A. M. Arjun, K. Rajendran, S. Pathan and P. A. Rasheed, *Anal. Methods*, 2023, **15**, 587–595.
44 R. Ye, Y. Liu, Z. Peng, T. Wang, A. S. Jalilov, B. I. Yakobson, S.-H. Wei and J. M. Tour, *ACS Appl. Mater. Interfaces*, 2017, **9**, 3785–3791.
45 D. H. Kweon, M. S. Okyay, S.-J. Kim, J.-P. Jeon, H.-J. Noh, N. Park, J. Mahmood and J.-B. Baek, *Nat. Commun.*, 2020, **11**, 1278.
46 J. Mahmood, F. Li, S.-M. Jung, M. S. Okyay, I. Ahmad, S.-J. Kim, N. Park, H. Y. Jeong and J.-B. Baek, *Nat. Nanotechnol.*, 2017, **12**, 441–446.
47 Y. Ding, K.-W. Cao, J.-W. He, F.-M. Li, H. Huang, P. Chen and Y. Chen, *Chin. J. Catal.*, 2022, **43**, 1535–1543.
48 P. Shringarpure and A. Patel, *Inorg. Chim. Acta*, 2009, **362**, 3796–3800.
49 N. E. Mircescu, M. Oltean, V. Chiș and N. Leopold, *Vib. Spectrosc.*, 2012, **62**, 165–171.
50 M. S. S. Balula, I. C. M. S. Santos, J. A. F. Gamelas, A. M. V. Cavaleiro, N. Binsted and W. Schlindwein, *Eur. J. Inorg. Chem.*, 2007, 1027–1038.
51 M. Bledowski, L. Wang, A. Ramakrishnan, O. V. Khavryuchenko, V. D. Khavryuchenko, P. C. Ricci, J. Strunk, T. Cremer, C. Kolbeck and R. Beranek, *Phys. Chem. Chem. Phys.*, 2011, **13**, 21511–21519.
52 Y. Li, X. Liu, L. Tan, Z. Cui, X. Yang, Y. Zheng, K. W. K. Yeung, P. K. Chu and S. Wu, *Adv. Funct. Mater.*, 2018, **28**, 1800299.
53 R. Malik, V. K. Tomer, N. Joshi, T. Dankwort, L. Lin and L. Kienle, *ACS Appl. Mater. Interfaces*, 2018, **10**, 34087–34097.
54 R. Malik, N. Joshi and V. K. Tomer, *Coord. Chem. Rev.*, 2022, **466**, 214611.
55 X. Li, J. Zhang, L. Shen, Y. Ma, W. Lei, Q. Cui and G. Zou, *Appl. Phys. A*, 2009, **94**, 387–392.
56 M. Tong, J. Yang, Q. Jin, X. Zhang, J. Gao and G. Li, *J. Mater. Sci.*, 2019, **54**, 10656–10669.
57 H. Xu, T. Zhang, Y. Gu, X. Yan, N. Lu, H. Liu, Z. Xu, Y. Xing, Y. Song, Z. Zhang and M. Yang, *Microchim. Acta*, 2020, **187**, 163.
58 S. Gong, Z. Jiang, S. Zhu, J. Fan, Q. Xu and Y. Min, *J. Nanopart. Res.*, 2018, **20**, 310.
59 J.-S. Li, Y.-J. Tang, C.-H. Liu, S.-L. Li, R.-H. Li, L.-Z. Dong, Z.-H. Dai, J.-C. Bao and Y.-Q. Lan, *J. Mater. Chem. A*, 2016, **4**, 1202–1207.
60 K. Wang, Q. Chen, Y. Hu, W. Wei, S. Wang, Q. Shen and P. Qu, *Small*, 2018, **14**, 1802132.
61 Y. Feng, P. Huang, Z. Zhou, X. Ding, L. Liu, X. Liu and J. Kang, *Nanoscale Res. Lett.*, 2019, **14**, 86.
62 J. Wojciechowska, E. Gitzhofer, J. Grams, A. M. Ruppert and N. Keller, *Materials*, 2018, **11**, 2329.
63 H. Wang, C. Wang, Y. Yang, M. Zhao and Y. Wang, *Catal. Sci. Technol.*, 2017, **7**, 405–417.
64 L. Wang, B. Wu, W. Li, S. Wang, Z. Li, M. Li, D. Pan and M. Wu, *Adv. Biosystems*, 2018, **2**, 1700191.
65 W. Feng, Y. Ding, Y. Liu and R. Lu, *Mater. Chem. Phys.*, 2006, **98**, 347–352.
66 S.-M. Wang, L. Liu, W.-L. Chen, E.-B. Wang and Z.-M. Su, *Dalton Trans.*, 2013, **42**, 2691–2695.
67 D. Xu, W.-L. Chen, J.-S. Li, X.-J. Sang, Y. Lu, Z.-M. Su and E.-B. Wang, *J. Mater. Chem. A.*, 2015, **3**, 10174–10178.
68 Y. G. Shen and Y. W. Mai, *J. Mater. Res.*, 2000, **15**, 2437–2445.
69 Y. Zhao, W. Hu, Y. Xia, E. Smith, Y. Zhu, C. Dunnill and D. H. Gregory, *J. Mater. Chem.*, 2007, **17**, 4436–4440.
70 B. Sivaranjini, R. Mangaiyarkarasi, V. Ganesh and S. Umadevi, *Sci. Rep.*, 2018, **8**, 8891.
71 U. Joshi, S. Malkhandi, Y. Ren, T. L. Tan, S. Y. Chiam and B. S. Yeo, *ACS Appl. Mater. Interfaces*, 2018, **10**, 6354–6360.
72 L. Peng, L. Su, X. Yu, R. Wang, X. Cui, H. Tian, S. Cao, B. Y. Xia and J. Shi, *Appl. Catal., B*, 2022, **308**, 121229.
73 E. V. Miu, J. R. McKone and G. Mpourmpakis, *J. Am. Chem. Soc.*, 2022, **144**, 6420–6433.
74 J. Park, S. Lee, H. E. Kim, A. Cho, S. Kim, Y. Ye, J. W. Han, H. Lee, J. H. Jang and J. Lee, *Angew. Chem., Int. Ed.*, 2019, **58**, 16038–16042.
75 Y. Wang, S. Yun, J. Shi, Y. Zhang, J. Dang, C. Dang, Z. Liu, Y. Deng and T. Yang, *J. Colloid Interface Sci.*, 2022, **625**, 800–816.
76 X.-L. Wang, Y. Tian, Z.-H. Chang and H. Lin, *ACS Sustainable Chem. Eng.*, 2020, **8**, 15696–15702.
77 C. Yue, N. Liu, Y. Li, Y. Liu, F. Sun, W. Bao, Y. Tuo, Y. Pan, P. Jiang, Y. Zhou and Y. Lu, *J. Colloid Interface Sci.*, 2023, **645**, 276–286.
78 A. A. Ensafi, E. Heydari-Soureshjani and B. Rezaei, *Int. J. Hydrogen Energy*, 2017, **42**, 5026–5034.
79 L. Men, T. Shi, J. Li, X. Li, B. Sun, Q. Pan and Z. Su, *Int. J. Hydrogen Energy*, 2022, **47**, 27452–27459.
80 J.-Y. Han, S.-H. Cai, J.-Y. Zhu, S. Yang and J.-S. Li, *Chem. Commun.*, 2022, **58**, 100–103.
81 H. Liu, G. Tan, M. Li, Z. Zhang, M. Getaye Sendeku, Y. Li, Y. Kuang and X. Sun, *Chem. Eng. J.*, 2023, **458**, 141414.
82 L. Wang, A. Wang, Z.-Z. Xue, J.-X. Hu, S.-D. Han and G.-M. Wang, *Inorg. Chem.*, 2022, **61**, 18311–18317.
83 S. Shahsavarifar, M. Masteri-Farahani and M. R. Ganjali, *Langmuir*, 2022, **38**, 12124–12131.
84 P. S. Kumar and P. Prakash, *J. Environ. Chem. Eng.*, 2023, **11**, 109045.